

Tunable collective behavior in active cytoskeletal assemblies

Simon L. Freedman, Shiladitya Banerjee, Glen M. Hocky, Aaron R. Dinner

Abstract

Cells can modulate the mechanical properties of the actin cytoskeleton in remarkable ways to maintain structural integrity, move and divide. This behavior is achieved through crosslinking proteins and bundling agents that dynamically control cellular structure, as well as active motors that generate active stresses and regulate intracellular transport. *In vitro* model systems using a small subset of purified proteins have revealed the minimal components necessary to confer this wide range of mechanical behaviors. Here, we take the same approach using agent-based computational modeling, and investigate the collective dynamics of disordered cytoskeletal assemblies, consisting of semi-flexible filaments, dynamic crosslinkers, and molecular motors. By tuning the properties of individual cytoskeletal elements, such as filament length, crosslinker stiffness, or motor kinetics, we explore the collective phases of actomyosin networks across dynamic regimes inaccessible to experiments. Our work elucidates the diverse pathways for cytoskeletal contractility, polarity organization, and molecular transport, and provides testable predictions for future experiments on reconstituted cytoskeletal assemblies.

1 Introduction

The actin cytoskeleton serves as a dynamic scaffold that allows eukaryotic cells to actively change shape, move, and adapt to their micro-environment. Although the cellular cytoskeleton constitutes a complex network of protein-protein interactions, *in vitro* model systems have revealed the minimal set of components required to exhibit a wide range of active mechanical behaviors including contractility and polarity organization [?, ?, 1]. In this work, we investigate the range of collective behaviors accessible to a minimal system consisting of cytoskeletal filaments, crosslinking proteins, and active molecular motors. Many groups have produced remarkable results using systems consisting only of these components, but a necessary limitation in those studies is the difficulty to control precisely some of the properties of constituents in the system. For example, filament stiffness, filament length, crosslinker length, and crosslinker affinity are all important biological parameters which vary in cells in complex and often coupled manner. The goal of this work is to present a mathematical model, in the form of a non-equilibrium molecular dynamics simulation, that can efficiently explore the phase space of this actin, myosin, and crosslinker system. This mathematical model can guide our understanding of the relationship between the microscopic biochemical protein-protein interactions and the macroscopic mechanical functionality of the ensemble. Additionally, because the model simulates actin, myosin, and crosslinkers in space and time, it will enable us to learn the trajectory of an ensemble, and how intermediate mesoscopic structures tune network functionality.

Extensive research illuminated the behavior of myosin in muscle cells, where actin filaments are arranged in parallel bundles termed sarcomeres; a bundle of myosin heads walks

towards the barbed end of two anti-parallel actin filaments and the resulting tension produces muscle contraction [2]. However, in the cytoskeleton of nonmuscle cells, there is no inherent ordering of actin or myosin filaments, so while interactions between individual myosin and actin filaments exist, how they act in concert to produce a variety of behaviors is an active area of research [1,3,4]. Recent experimental studies [1,5] have reconstituted networks of actin and myosin, and analyzed how changing their respective concentrations and lengths, can effect the ability of a disordered ensemble to contract and form static structures. They have also incorporated various actin binding proteins (crosslinkers) into their experiments such as filamin, scruin, and α -actinin, as these control network connectivity, and are instrumental in crosslinking actin filaments to form long lasting, force propagating bundles and networks [1,4–6]. The goal of all of these experiments is to develop a phase diagram that shows the importance of key players of active networks, such as myosin density [1], actin bundle rigidity [1], and cross-linker density [5] in structure formation and force generation within the cytoskeleton.

For example, by varying the density of myosin added to a reconstituted actin network, one can vastly effect its biomechanical behavior. At low motor density, the myosin will translocate large distances but will not cause the network to contract [7]. Above a critical density, the myosin will contract the network and raising the density further will result in more extensive contraction. However, there also appears to exist a second critical density past which more motors are ineffective at increasing contractility [5]. These *in vitro* experiments have also been used to probe the underlying mechanisms that control the ensemble network behavior. To date, results strongly suggest that actin filament buckling and severing as well as relative actin and myosin sliding are all necessary for network contraction [1,5].

To probe the microscopic origin of these complex behaviors, we have developed a simulation model, motivated both by *in vitro* experiments as well as several previous computational models of actin and myosin. Some of these models were designed to understand rheological properties of crosslinked actin networks [8–11], some have been focused on the ensemble motion of motors with respect to filaments [3,12,13], while others have aimed at understanding larger, structure related questions, such as how disordered assemblies of filaments and motors collectively form asters [14] or contract [15–18]. Our model is constructed by including many of the best features of these preceding models. We will use the potential energy for an actin filament as described by Head et al., for simulating actin filaments that can both bend and stretch, and also initialize our networks similarly, by placing crosslinkers at intersections to form well connected networks. In contrast to references [9,16], we will simulate non-equilibrium dynamics, including fluctuations due to non-zero temperature, cross-linkers and myosins binding and unbinding, and the processive activity of myosin. We have used predictions from [3] to extrapolate numerical parameters for the binding kinetics of a myosin mini-filament as they relate to a single myosin head. Force propagation rules and binding kinetic equations will be similar to those of [12,14] with slight differences in how we actually simulated the fluctuating filaments.

In this work, we show that this model is well bench-marked to reproduce known experimental results for actin filaments, ensembles of actin and crosslinkers (passive networks), and ensembles of actin and myosin (active networks). At the polymer level, we will reproduce predicted spatio-temporal fluctuations of actin filaments. For passive crosslinked networks we will reproduce known stress strain relationships. For active networks, we will reproduce well-understood velocity distributions of actin filaments in a myosin motility assay. These results demonstrate that it is possible to capture many key properties of cytoskeletal networks within a single model which has not been optimized to reproduce any particular set of experiments.

We then show that these simulations predict non-trivial emergent dynamical behaviors which are tunable based on the properties of the filaments, crosslinkers and motors involved.

We find that crosslinker affinity modulates filament bundling and network coarsening in a non-monotonic manner. We show that crosslinker stiffness governs the strain stiffening response of these networks in a simulated rheology experiment.

We introduce motors into our networks and demonstrate how ensembles of randomly oriented actin filaments and crosslinkers can be rearranged by myosin motors to form tunable structures with distinct biophysical and mechanical functionality. We show that motor-dependent contraction produces polarity sorted networks and predict how that behavior depends on the concentration of motors. We use these results to interpret emergent contractility as a competition between bundling and polarity sorting. Finally, we study how varying the filament length, motor density, and motor-filament binding affinity can change the way in which the motors work in concert to translocate actin filaments, which may have implications for how to optimize the rate at which behaviors such as polarity sorting and contractility would be observed.

2 Results

The most striking biological function of actomyosin networks is their contractility, which results in muscle cell contraction, and is instrumental in motility and division in non-muscle cells. That these complex macroscopic mechanisms arise stochastically from simple microscopic interactions suggests the ability to engineer materials with controllable network topologies and dynamics. Recently, in-vitro experiments of reconstituted actomyosin networks have demonstrated this controllable architecture by varying motor density and crosslinker density and showing how they effect contractility [1, 5]. Our model shows a similar dependence of contractility on motor density. Additionally, we show that we can tune two different macroscopic organizational techniques: bundling, in which dynamics crosslinkers pin filaments into robust networks, and polarity sorting, in which motors align filaments by their polarity.

In the interest of computational efficiency we have chosen to coarse grain actin filaments, and crosslinker proteins at length scales relevant for network behavior. Actin filaments are modeled as polar worm-like chains (WLC) such that one end of the chain represents the barbed end of a filament and the other end represents its pointed end. Crosslinkers are modeled as Hookean springs such that both ends of the spring (heads) can bind and unbind from filaments. Experiments have shown that adding crosslinkers to assemblies of F-actin yields actin bundles [1, 5, 6] and that increasing crosslinker density can increase the length scale of contraction [1]. Our results show that varying the stiffness of these springs changes the rheology of an assembly of crosslinkers and filaments, while varying the binding affinity effects the magnitude of actin bundling.

We parameterized our model in $2D$ similar to the nearly flat in vitro reconstitutions of actomyosin, as this setup is sufficient to reproduce structures of biological interest, and allows us to simulate larger systems for longer times. Because we use a $2D$ system to represent a $3D$ experiment, we exclude the steric interactions of filaments and crosslinkers, to account for some of the freedom lost from the reduction in dimensionality.

2.1 Crosslinkers and filaments form bundled networks

The rapid binding and unbinding of crosslinking proteins from actin filaments can reorganize initially disordered filaments into thickly bundled networks. This behavior is distinct from motor-driven contractility, because the overall network structure changes, without explicit force dipoles to strain and buckle filaments. We have found that we can tune this bundling mechanism

by changing the crosslinker-filament binding affinity.

To demonstrate this behavior, thirteen simulations were initialized with 500 $15\mu m$ worm-like-chain filaments scattered on a $75\mu m \times 75\mu m$ simulation cell, and $0.15\mu m$ crosslinkers doubly bound at filament-filament intersections. The assemblies then evolved via Brownian dynamics for 200s. Each simulation had a different dissociation rate for crosslinkers k_{off}^{cl} varying logarithmically between $0 - 1800 s^{-1}$. The results are shown in Figure 2.

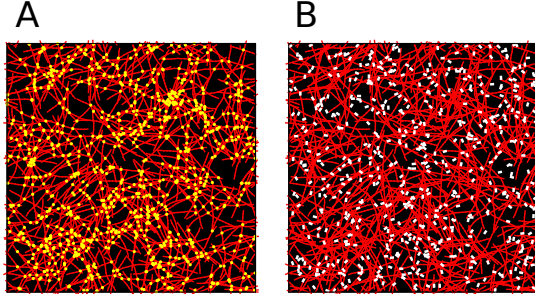


Figure 1: Initial configuration of actin filaments (red) for (A) assemblies which initially have crosslinkers (yellow, one third shown) placed at intersections and (B) assemblies with motors $\rho_m = 0.1\mu m^{-2}$ (white) scattered throughout.

The magnitude of bundling was measured by the radial distribution function of actin filaments, $g(r) = P(r)/(2\pi r \delta r \rho)$ where $P(r)$ is the probability that two beads on different filaments are a distance r , $\delta r = 0.05\mu m$ is the bin size and $\rho = 500/(75\mu m)^2$ is the number density. As seen in Figure 2 C-D, the relationship between k_{off}^{cl} and $g(r)$ is non-monotonic. A disassociation rate that is too low will not allow for significant restructuring from the initially random configuration, and a disassociation rate that is too high will not yield stable structures. However, at intermediate values of k_{off}^{cl} , a stable, thickly bundled network can be formed.

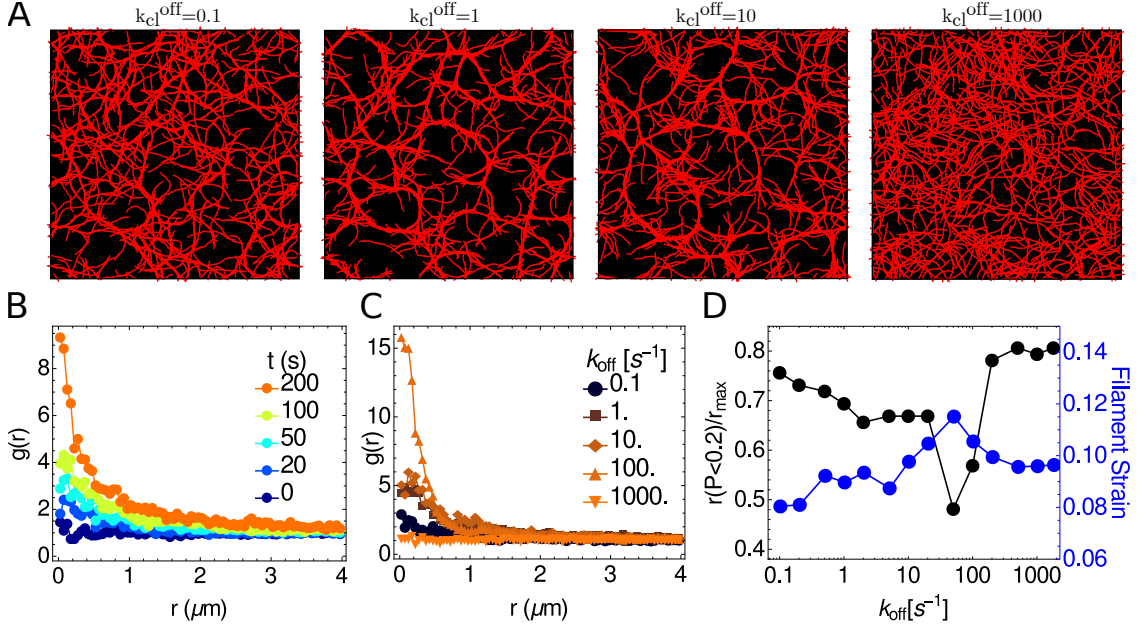


Figure 2: (A) Actin filament (red) assemblies after $t = 200\text{s}$ for varying disassociation constants. Filaments in red. (B) Radial distribution function of beads on an actin filament for the $k_{cl}^{off} = 20\text{s}^{-1}$ at various times throughout the simulation. As the simulation proceeds, the higher peak at lower r values shows the bundling increasing. (C) Radial distribution function of actin filaments at $t = 200\text{s}$ for varying k_{cl}^{off} . The curves show non-monotonic behavior, as both high and low k_{cl}^{off} have a shorter correlation distance than curves with mid-range k_{cl}^{off} . (C) We measure this monotonicity by marking the distance at which 80% of the area under the curves in (B) are covered. Lower values mean longer decorrelation lengths, indicating a larger magnitude of bundling. We also show that the difference in filament strain across these simulations is minimal, less than 0.025, and shows no clear relationship with the radial distribution functions. Contrast this with contracting networks in Figure 6, where where filament strain ranges from 0 to 0.35 and correlates with network divergence.

2.2 Strain stiffening behavior of crosslinked networks is tunable

The material properties of cross-linked F-actin networks are generally characterized using rheology. In a common experiment, actin and crosslinker proteins are mixed and form a crosslinked mesh. The mesh is placed in a rheometer and then sheared by a prestress σ_0 . The prestressed network then undergoes a sinusoidal differential stress of magnitude $d\sigma \ll \sigma_0$. By measuring the resulting strain, one can calculate the differential elastic modulus $G(\sigma_0) = \frac{d\sigma}{d\gamma}$. In experiments using a stiff crosslinker, such as scrulin, the dependence of the differential modulus on high prestress is $G \propto \sigma_0^{3/2}$, indicating that this shear stiffening is a direct result of the nonlinear response of stretching actin [6, 19]. Experiments using more compliant crosslinkers, such as filamin, have found a softer stiffening response, $G \propto \sigma_0$, indicating that a significant amount of stress is going into the crosslinkers, and not the actin [20].

These results suggest that the shear stiffening behavior of a crosslinked network can be tuned by varying the crosslinker stiffness. To test this possibility, the configuration of filaments shown in Figure 1 was reproduced with varying crosslinker stiffness k_{cl} . To inhibit network restructuring, the detachment rates of the crosslinkers was set to zero. An affine strain of $\delta\gamma = 0.001$ was applied such that the horizontal position of every actin bead (x_a) was shifted

$$x_a \rightarrow x_a + \delta\gamma \left(\frac{y_a}{Y} \right) \quad (1)$$

following the overdamped SLLOD equations of motion [21]. The periodic boundary was simultaneously shifted following the Lees-Edwards convention [22]. The mesh was then allowed to relax for $t_{relax} = 0.001s$ before the next strain of γ . This was performed for $T_f = 0.5s$ so that the total strain was $\gamma T_f / t_{relax} = 0.5$. Increasing t_{relax} did not significantly change the simulation results as seen in Figure S2(a).

The strain stiffening scaling for each crosslinker stiffness was measured by calculating w , the strain energy density at each timestep

$$w(t) = \frac{1}{XY} \left(\sum_f U_f + \sum_{cl} U_{cl} \right) \quad (2)$$

where U_f is defined in Section 4.1 and U_{cl} is the potential energy of each cross link, and averaging over windows of size t_{relax} to obtain $w(\gamma)$. Figure 3 shows the results of these calculations for various values of crosslinker k_{cl} . By varying the ratio of filament to crosslinker stiffness, we were able to vary the power law scaling of the strain energy density with respect to the strain. For extremely low k_{cl} , the sheared networks behaved as $w \propto \gamma$ or $G = \frac{d^2 w}{d\gamma^2} = 0$ as if the network had no resistance to shear, while for high k_{cl} , $w \rightarrow \gamma^4$. Thus, one can tune the behavior of these networks from being liquid-like, with $w \propto \gamma$, through the elastic solid regime of $w \propto \gamma^2$ as well as strain stiffening regimes of $w \propto \gamma^3$ and $w \propto \gamma^{3.5}$ observed in experiment [6, 20].

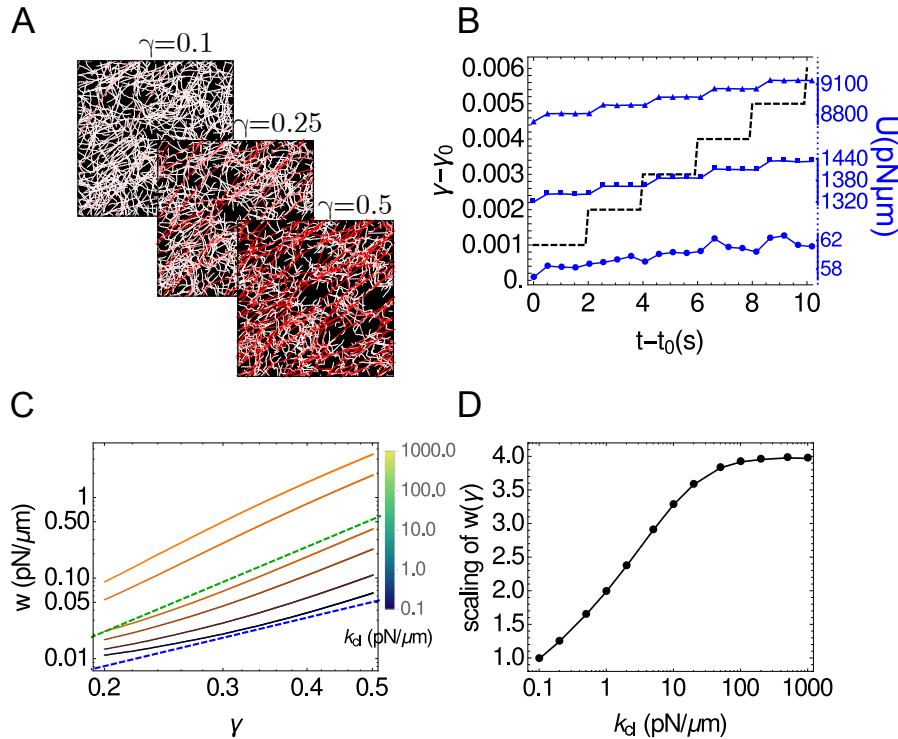


Figure 3: (A) Snapshots of a strained network ($k_a = k_{cl} = 1000$) at $t = 0.1s$, $t = 0.25s$ and $t = 0.5s$. Color indicates stretching energy on each link, with white being the lowest and red being the highest. (B) The potential energy of the network as a function of time shown at different strains $\gamma_0 = 0.1$ (circles), $\gamma_0 = 0.25$ (squares) and $\gamma_0 = 0.4$ (triangles) where $t_0 = \gamma_0 \times 1s$. Black dashed line shows the strain. (C) Strain energy density ($w = U/\text{area}$) for various values of crosslinker stiffness k_{cl} . Blue dashed line indicates expected behavior for an elastic solid $w \propto \gamma^2$ and green dashed line indicates strain stiffening behavior of $w \propto \gamma^{3.5}$ as observed in [6, 19]. (D) Power law of w , evaluated via least squares fit to $\ln(\gamma)$ vs $\ln(w)$.

2.3 Motors sort filaments

Motors are modeled as crosslinkers with the caveat that a head bound to a filament will process toward the filament's barbed end (see Section 4.3 for a full description). This implementation allows for filament sliding and filament buckling, as seen in Figure 4, both of which are instrumental for actomyosin contractility [1]. In large networks, motors can perform these mechanisms, as well as translocate across filaments, and increase network connectivity [5].

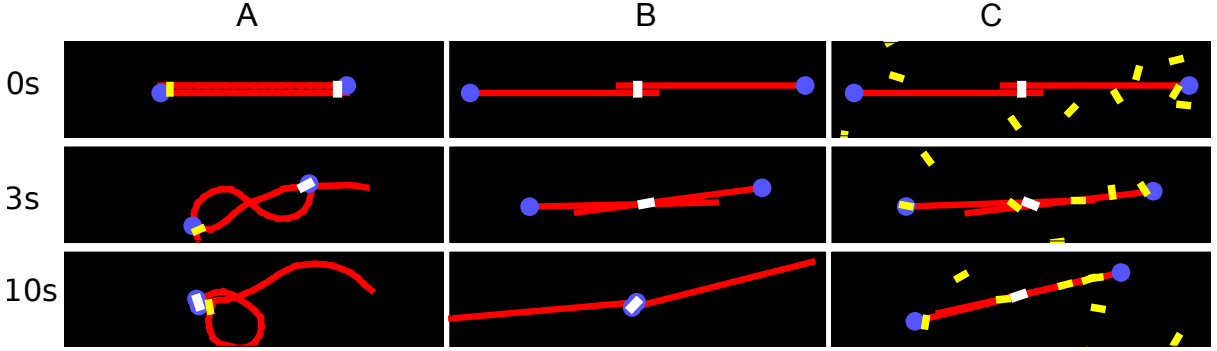


Figure 4: Time series of three antiparallel $10\mu\text{m}$ filaments (red) interacting with a minimal set of motors (white) and crosslinkers (blue) for 10s . Barbed ends of filaments are marked by a blue dot. (A) Filaments are semiflexible (21 bead-spring chain) and pinned on the left by a crosslinker, so the motor-filament interaction yields contraction via buckling. (B) Filaments are rigid (2-bead-spring chains) and unpinned, so motor-filament interaction yields that filaments are slid past each other. Thus, they transition from an initially extended state, to a contracted state at $t = 3\text{s}$ and back to an extended state at $t = 10\text{s}$. (C) Same as (B) but with a population of crosslinkers near the filaments that stabilize the system in the contracted state.

To isolate the role of active motors on assemblies of semiflexible filaments, the actin assembly in Figure 1 was generated without crosslinkers at filament intersections, but with $0.5\mu\text{m}$ motors were scattered uniformly throughout the simulation cell. In these simulations, the motor duty ratio was kept near unity to replicate the behavior of a myosin minifilament, while the density of motors was varied between simulations.

The results, shown in Figure 5, indicate that at higher motor densities, filaments were sorted by polarity, but were not clustered. Motors aggregated on the barbed ends of filaments and thereby brought the barbed ends together, to form asters. The magnitude of polarity sorting was measured by calculating the average distance of a bound motor from the barbed end of filament to which it was bound. As seen from Figure 5 A-B, increasing motor density had the effect of decreasing this distance, indicating a larger magnitude of polarity sorting. It appears therefore that this form of restructuring is highly tunable.

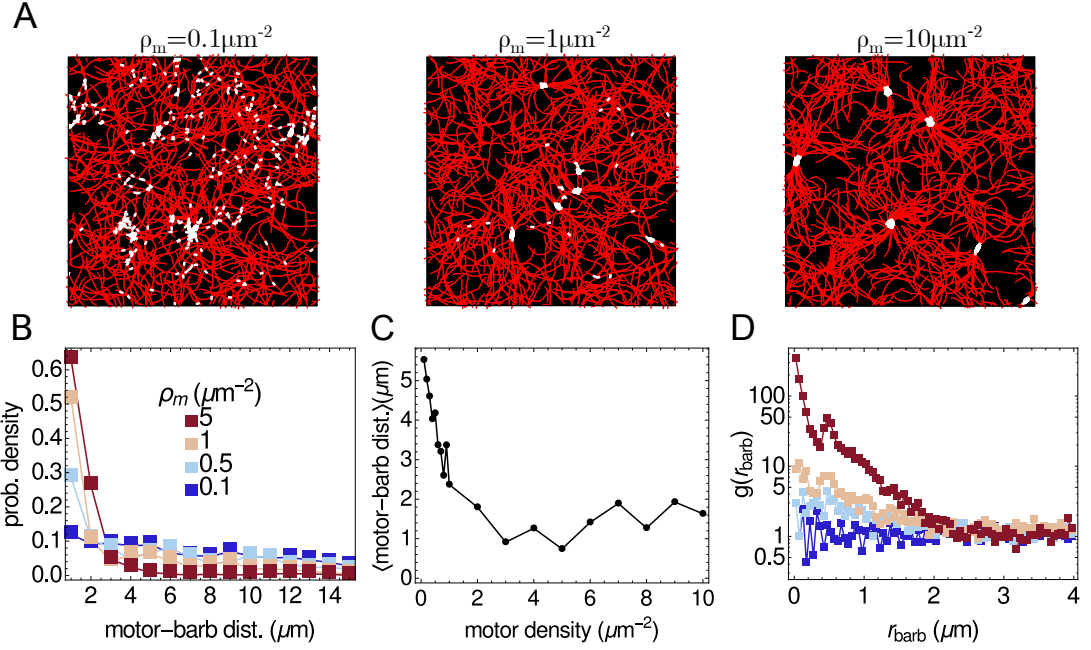


Figure 5: (A) Networks at their polarity sorted end configuration ($t = 96\text{s}$). Filaments in red, motors in white. A maximum of 1000 motors are shown in each case. (B) Histograms of the distance of an attached motor head from the barbed end of the filament to which it is attached for varying motor density at $t = 96\text{s}$. (C) The average distance of a motor head from the barbed end as a function of motor density. (D) Radial distribution function for barbed ends shows a strong dependence on motor density. For $\rho_m = 5\mu\text{m}^{-2}$, a peak is also visible at the motor rest length $l_m = 0.5\mu\text{m}$.

2.4 Contractility emerges from competition between bundling and polarity sorting

When both crosslinkers and motors are combined with semiflexible filaments, the assemblies become contractile. To demonstrate this behavior, actin filament assemblies were initialized to the configuration in Figure 1 with crosslinkers at their intersections with motors scattered uniformly throughout the cell. The motor density varied between simulations from $0.1 - 10\mu\text{m}^{-2}$. The crosslinkers were kept sticky with a low duty ratio, while the motors were highly active with a high duty ratio. This ensured that connectivity of the network was almost exclusively controlled by crosslinkers while force generation was controlled by motors.

The results of these networks can be seen in Figure 6. The effective contractility was measured by interpolating a velocity field from the displacement vectors of filament beads, and measuring the divergence of the velocity fields as is done in ref [5]. A negative divergence indicates a contractile network. As evident in Figure 6(B), higher motor density leads to larger contractility. Figure 6(D) shows that actin buckling, here measured as the change in the end to end distance s of an actin filament

$$s = \left(1 - \frac{|r_{15} - r_0|}{\sum_{i=1}^{15} |r_i - r_{i-1}|} \right) \quad (3)$$

correlates with contractility, suggesting that the primary mechanism driving contractility in these flexible networks is buckling, as seen in experiment [1].

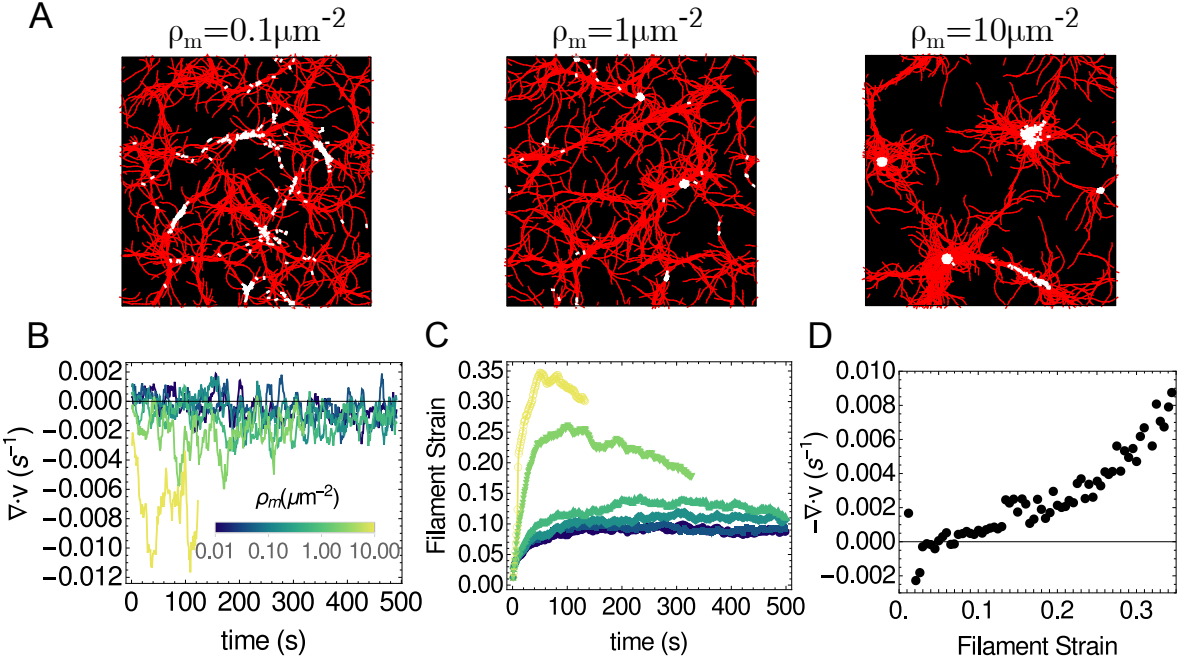


Figure 6: Assemblies with motors and crosslinkers yield contraction. (A) Networks at their largest contractility for different motor densities. Filaments in red, motors in white. Only 1000 motors are shown in each case. (B) Average divergence as a function of time for networks of varying motor density. Networks with a higher density of motors are more contractile. (C) Average filament strain (defined in Equation (3)) as a function of time for the same networks. (D) Correlation between filament strain and network strain (measured as negative of divergence for all times and all motor densities, averaged over bins of size 0.005)

2.5 Modulating ensemble motor behavior

While the force dependent detachment and speed of an individual myosin motor is well approximated by the input behavior described in Section 4.3, the ensemble behavior of many myosins is not input, and could provide a benchmark that the simulation is accurately representing active actomyosin assays [23]. One experiment involving an ensemble of motors is the motility assay, in which a layer of myosin is adhered to a plate, and actin filaments are placed on top of the myosin. Because the myosin cannot diffuse, they instead slide the actin filament across the assay. Although this experiment typically involves single myosin heads, and not myosin minifilaments, we believe that functionally the situations would be equivalent, with the substitution that each model motor head approximates the activity of dozens of single molecule myosin heads. Various groups [24, 25] found a nonlinear dependence of the speed of an actin filament across the assay on the concentration of myosin, the length of the actin filament, and the concentration of ATP in the sample. By allowing filaments to interact with more motors, one can increase the filament monotonically to a critical speed.

To explore this experiment, we randomly distributed motors on a $(50 \mu\text{m})^2$ periodic simulation cell and constrained one head of each motor to remain in place. Filaments were also placed in the simulation cell and allowed to interact with the unconstrained motor heads. The number of motor-filament interactions was manipulated in three ways: by varying the motor concentration ρ_m , the filament contour length L , and the duty ratio $r_D = k_m^{on}/(k_m^{on} + k_m^{off})$. The results are shown in Figure 7, where we have used the dimensionless parameter $\rho_m L^2 r_D$ to describe the various experiments.

In general, the findings were qualitatively similar to the experimental results. For low motor

density, filament length and duty ratio, transverse filament fluctuations dominate over longitudinal motion as the filament is not being propelled by motors faster than diffusion. However, as these variables are increased, longitudinal motion dominates. This can be seen from the mean squared displacement, plotted in Figure 7(D), where low $\rho L^2 r_D$ yields diffusive behavior with an $\langle r^2 \rangle \propto t$, and the motion becomes ballistic with $\langle r^2 \rangle \propto t^2$ as $\rho L^2 r_D \propto 100$. The speed of this motion plateaus at $v_{||} \approx 1\mu\text{m}/\text{s}$ which is the average unloaded motor velocity, as seen in experiment. Figure 7(C) shows that aside from being propelled, filaments are also buckled in the presence of a large number of motors, as filament strain increases with increasing $\rho_m L^2 r_D$. Although there are no explicit crosslinkers, at a high enough concentration, motors near the barbed end of a filament will pin the filaments for a short time, and induce buckling the same way crosslinkers do in contractile networks.

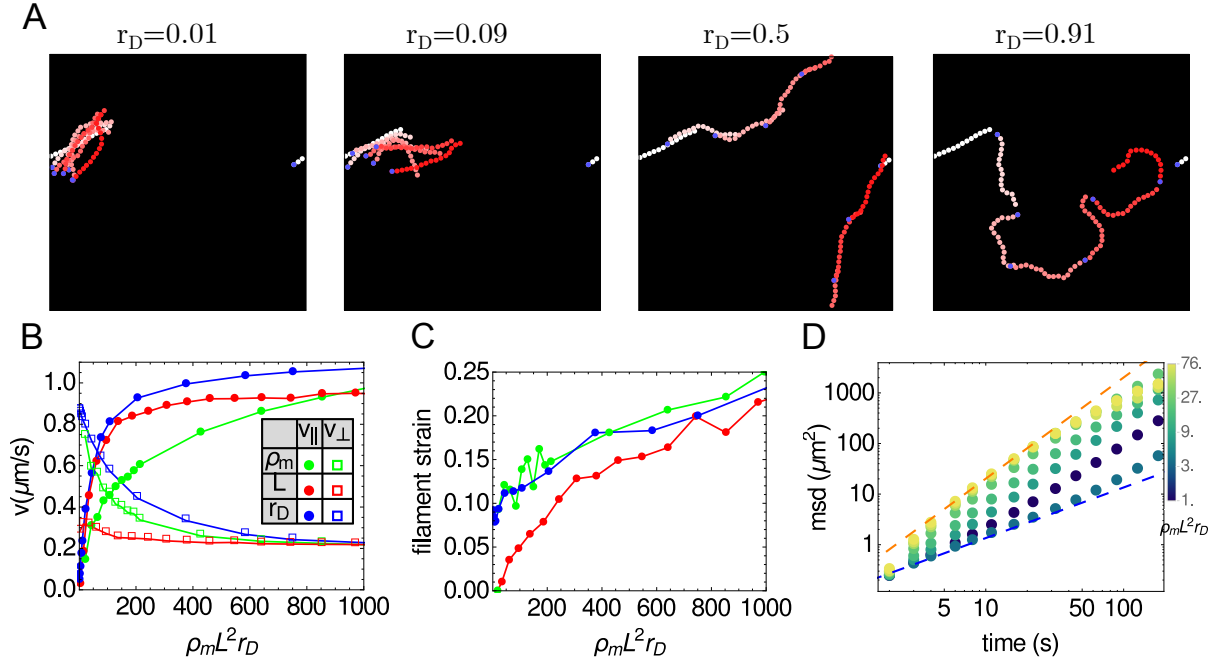


Figure 7: (A) Position of a filament for $\rho_m = 10\mu\text{m}^{-2}$ and $L = 16\mu\text{m}$ for different values of the duty ratio. White filament is $t = 0$ and dark red is $t = 90\text{s}$. Blue dot marks the barbed end of filaments. (B) Longitudinal filament speed (circles) monotonically increases to a plateau while transverse speed (squares) decreases with larger motor density, filament length, and duty ratio. Green: ρ variable, $L = 15\mu\text{m}$, $r_D = 0.95$; Red: $\rho_m = 4\mu\text{m}^{-2}$, L variable, $r_D = 0.95$; Blue: $\rho_m = 10\mu\text{m}^{-2}$, $L = 15\mu\text{m}$, r_D variable. (C) Filament strain, defined in Equation (3), as a function of dimensionless parameter, indicates that while the motor is being propelled by motors, it also is being buckled. (D) Mean squared displacement for various values of $\rho_m L^2 r_D$ shows that the transition from diffusive (blue dashed line) to ballistic (red dashed line) behavior occurs at low values of this parameter.

3 Discussion

The goal of this paper is to introduce a framework that could accurately and efficiently simulate active networks of F-actin, myosin, and crosslinker proteins to explore the various structural phases that this system can produce. In doing so, we have shown that our model can reproduce the key results of canonical actomyosin experiments. When simulated networks were sheared, strain stiffening was observed and filament speed scaling in simulated motility assays matched experimental results. Networks with dynamic crosslinkers were shown to form bundles, and

networks with motors and crosslinkers contracted. We have also expanded significantly on these experiments.

For crosslinked networks, we showed that the scaling of strain stiffening can be tuned by changing the crosslinker stiffness. Many other models have successfully studied the viscoelastic properties of crosslinked actin networks [8–11]. For example, Head, et al., used a similar simulation to ours but with straight rod filaments, and bending potentials at rod intersections, and was able to identify three elastic regimes, characterized by the mean distance between crosslinkers and the temperature [9]. Similar models used non-Hookean crosslinkers to show how unfolding can yield strain softening at large strain [26]. Others 3D models, with explicit filament bending have examined the frequency dependence of these networks and reproduced theoretical predictions [11, 27, 28]. Our contribution in this area is that we have shown that by modeling crosslinkers as idealized Hookean springs, and varying their stiffness, one can change the scaling of strain stiffening. This is particularly interesting, given that recent experimental findings suggest that one can engineer actin binding proteins of varying stiffness [29].

The ensemble motion of a many myosin motors with respect to a single actin filament has also been studied via simulation, in order to develop a realistic model of a myosin minifilament. Erdmann and Schwarz, who used Monte Carlo simulations to verify a master equation that expresses the probability that N motors are bound at time t to a single filament [13] were able to make accurate predictions for the duty ratio and force velocity curves for myosin minifilaments. Stam et al. used simulations to study force buildup on a single filament by a multi-headed motor and found distinct timescale regimes over which different biological motors could exert force and act as crosslinkers [3]. These models of actin-myosin interaction are important to understand the mechanics at the level of a single filament, and their results can be incorporated into larger network simulations. However, our results show that even a minimal model of actin and myosin is able to capture the ballistic, longitudinally processive behavior of actin filaments in a motility assay seen in experiments.

Other actomyosin models have explored the driving mechanisms behind contractility. Dasanyake, et. al., extended the model in [9] to include a term in the potential energy that corresponded to myosin motor activity, and observed the emergence of force chains that transmit stress throughout the network [16]. Wang and Wolynes [15] model the F-actin networks as a graph of crosslinkers (nodes) and rigid actin filaments (edges) in which myosin motor activity is simulated via antisymmetric kicks along the filaments and predict a binary phase diagram of networks which are either contractile or not as a function of cross linker and myosin densities. While the simplicity of these models is intriguing, they do not account for explicit filament buckling, and their integration is performed via Monte Carlo, more applicable to structure formation than dynamics. We have shown that using an agent based model we can reproduce the experimentally observed contractility of actomyosin networks, that it scales with motor density, and that it correlates with filament buckling, both of which have been confirmed in *in vitro* reconstitutions [1, 5].

Contractility and structure formation has also been explored in the context of agent based models. Nedelec used dynamic simulations of ensembles of filaments and motor proteins to explore aster formation in microtubule-kinesin assemblies, as well as motility and contractility in actomyosin [12, 18, 30]. Kim used an agent based approach of filaments, motors and crosslinkers, to explore a variety of topics, including bundling in crosslinked networks and force generation by myosin motors [17, 31]. While the bundling observed in [31] was the result of crosslinkers that explicitly bind parallel filaments, we have that generic crosslinking leads to network coarsening and that this bundling effect depends strongly, and non-monotonically on the crosslinker-filament affinity. These bundled networks have the important physical property

of being able to transmit forces large distances, and are thought to serve the biomechanical functionality of forming force chains to propagate stress throughout the cell.

Additionally, we showed that we can tune polarity sorting in filament assemblies. Polarity sorted networks can be used to by load-carrying motors to transmit cellular goods large distances, so insight into how a cell modulates this behavior could be extremely helpful in biophysics and active matter. While this polarity sorting is similar to the aster formation seen in [14,30], we have shown that the process will also occur when filaments are semiflexible, have developed a reliable order parameter for measuring this process, and shown that the magnitude of this parameter increases monotonically with motor density.

While our model is thorough in what it aims to simulate it is limited by a few experimental observations that are currently not implemented. First, the structure of myosin minifilaments is significantly more complex than a two headed spring. As mentioned, these minifilaments have dozens of heads, which allows them to walk along multiple filaments and could result in subdiffusive behavior [32] and significantly increase local network elasticity [33]. Another limitation of our system is that the actin filaments are static, and will not polymerize, depolymerize or sever. Within actomyosin assays it is clear that recycling of actin monomers and to a lesser degree, filament severing plays an important role in contraction [1]. Within the cytoskeleton, actin treadmilling is also important for shape production. Additionally, these simulations are all run in $2D$ and without steric interactions, and dimensionality and volume exclusion may play important roles. While we intend to address and investigate these limitations in future works, we believe that the successful benchmarking of the simulation at various levels is a significant argument in favor of the current setup.

There are still many unanswered questions regarding cytoskeletal actomyosin networks that we hope to addressed using this simulation, such as how they controllably reshape the cell membrane, and they form force propogating chains across the cytoskeleton. In particular, it is significantly easier to measure local forces and energies in simulation than in experiment, so we expect this model will aid the process of isolating the particular mechanisms involved in restructuring these polymer assemblies. We stress, however, that the applicability of such a simulation package reaches beyond studying the phases of actomyosin networks. We believe this simulation can shed light on a variety of active polymer assemblies.

Similar networks that involve other proteins also exist in the cytoskeleton, such as microtubule-kinesin-dynein networks and could be investigated using this simulation methodology. Furthermore, the cytoskeleton demonstrates how populations of simple machines can self assemble into active materials with useful mechanical properties, and one can use this simulation to efficiently design these types of self assembled materials. Thus, the non-equilibrium molecular dynamics framework of this simulation can be used to model and study many open questions in active matter and biophysics.

4 Methods

4.1 Actin Filaments

Actin filaments are treated as a worm-like chain, with each filament represented as a set of $N+1$ beads connected by N harmonic springs (links), with an additional harmonic angular potential applied on the $N - 1$ angles along the chain, as depicted in Figure 8(A). The linear springs penalize stretching of individual subunits and the $N - 1$ angular harmonic springs penalize bending and enforce the length scale over which the filaments are semi-flexible.

The internal forces on actin filaments can be obtained from the gradient of the potential energy U_f

$$U_f = U_{stretch} + U_{bend} \quad (4)$$

$$U_{stretch} = \frac{k_a}{2} \sum_{i=1}^N (|d_i| - l_a)^2 \quad (5)$$

$$U_{bend} = \frac{\kappa_B}{2l_a} \sum_{i=2}^N \theta_i^2$$

where $d_i = r_i - r_{i-1}$, $\theta_i = \arccos\left(\frac{d_i \cdot d_{i-1}}{|d_i||d_{i-1}|}\right)$, k_a is the stretching force constant, κ_B is the bending modulus, and l_a is the equilibrium length of a link.

For a confined semiflexible filament, it has been shown that for a polymer of a given persistence length L_p , the shortest length that should be considered as unbending (l_a) is given by $l_a \approx A^{2/3} L_p^{1/3}$ where A is a length scale associated with the confinement of the filament [34]. In these simulations, filaments were confined by nearby motors and crosslinkers. Since the smallest motor or crosslinker density used was $\rho_m = 0.1 \mu m^{-2}$, $A \geq 1/\sqrt{0.1 \mu m^{-2}} \Rightarrow l_a \geq 5 \mu m$. In general, we used $l_a = 1 \mu m$. The bending force constant is derived from the persistence length L_p such that $\kappa_B = L_p k_B T$ where k_B is Boltzmann's constant and T is the temperature [35]. Experimentally, the stretching force constant has been measured to be in the approximate range $k_a = 40 - 70 pN/nm$ [36, 37]; however, simulating a network of filaments with this large of a stiffness is computationally inefficient since the maximum timestep of a simulation is inversely proportional to the largest stiffness in the simulation. Therefore, we chose $\frac{\kappa_B}{l_a} \ll k_a$, so that the filaments were still much easier to bend than to stretch, enabling us to run simulations of experimentally relevant dimension. We show that our simple filament model exhibits expected behavior for a semiflexible filament in the next section and we have further verified that k_a did not effect the persistence length of the filament, as seen in Section 6.2.1.

Since actin bending is instrumental for actomyosin contraction, and simulating precise bending moduli is non-trivial, we tested our filaments by measuring spatial and temporal fluctuations and comparing with theoretical predictions. In a two dimensional WLC, a bending of two adjacent segments is expected to result in a local change in free energy of $\frac{\kappa_B}{2l_a \theta_i^2}$, and it is predicted that [38]

$$\langle \theta^2(l) \rangle = \frac{l}{L_p} \quad (6)$$

$$\langle \cos(\theta(l)) \rangle = \exp(-l/2L_p) \quad (7)$$

where $\theta(l) = \theta_j - \theta_i$ where $1 < i < j \leq N$, $l = l_a(j-i)$ and L_p is the persistence length. To test our model against these equations, we simulate 100 filaments of $L = 200 \mu m$ and $\kappa_B = 0.08 pN \mu m^2$ at $T = 300 K$ for $T_f = 100 s$ and measured the resulting filament configuration every 1s. We discard the first 10 seconds of each simulation to allow equilibration, and we used only the middle $150 \mu m$ of the filament to calculate these correlation functions. Figure S1(a) shows that the measured persistence length, obtained by performing a least squares fit to plots of $\log(\langle \cos(\theta(l)) \rangle)$ for various values of κ_B yields the expected result over at least 3 orders of magnitude. Further measurements of the persistence length as well as verifications of its independence on other filament parameters is available in the supplement Section 6.2.

An additional prediction for semiflexible filaments is the scaling of fluctuations with time. Fluctuations transverse to the filament orientation have been shown to increase as a function of time as $\langle dr_\perp^2 \rangle \propto t^{3/4}$ while longitudinal fluctuations have been shown to follow the power law

$\langle dr_{||}^2 \rangle \propto t^{7/8}$ [39]. To test these predictions, we followed the procedure outlined in [39] and generated $N = 100$ initial filament configurations of a $20\mu m$ filament. For each configuration we ran $M = 100$ simulations of the filament fluctuating for $1s$. At each time step we collected the $2N$ positions of the filament ends, $r_e(t)$. We then calculated the eigenvalues of the covariance matrix $cov(r_e(t) \cdot \hat{i}, r_e(t) \cdot \hat{j})$ where $i, j \in \{x, y\}$. The larger eigenvalue $\lambda_1(t)$ corresponds to the slower longitudinal fluctuations (i.e., $\lambda_1(t) \propto t^{7/8}$) while the smaller eigenvalue corresponded to the faster perpendicular fluctuations ($\lambda_2(t) \propto t^{3/4}$). We show in Figure 8(C) that our simulation exhibits scaling of these eigenvalues in good agreement with the prediction of Ref. [39].

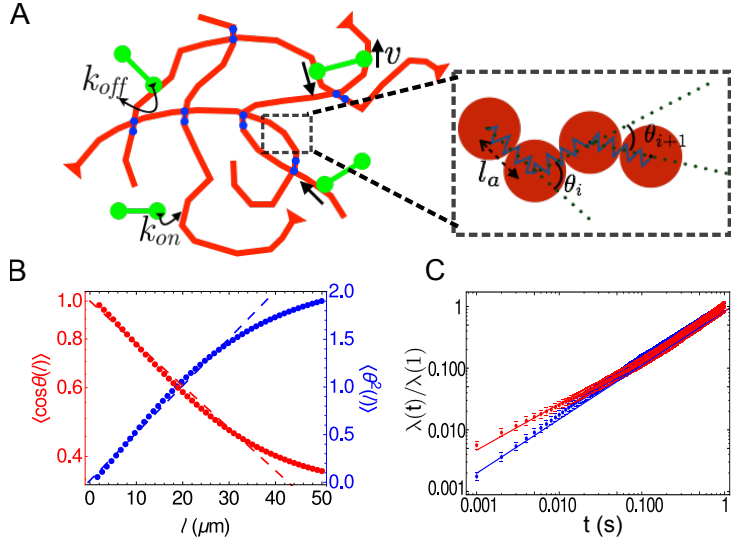


Figure 8: (A) Sketch of semiflexible filaments (red); motors (green) binding, unbinding, and walking; and crosslinkers (blue) connecting filament intersections. Zoom in of the filament model shows a segment of the bead spring chain, identifying the angle used in Section 4.1. (B) Decorrelation of tangent vectors (red dots) and fluctuations in angles between links (blue dots) as a function of the arc length between them. Red dashed line is $e^{-s/2L_p}$ shows the expected behavior from the input bending modulus of $0.08pN - \mu m^2$ and blue dashed line has slope $1/L_p$. (C) Eigenvalues of covariance matrices for the positions of endpoints of filaments as a function of time. We analyze fluctuations of $N = 100$ filaments, with each point the average over the $2N$ eigenvalues for $\lambda_1(t)$ and $\lambda_2(t)$ and error bars showing the standard deviations for the distribution of these values. Blue dots shows the longitudinal fluctuations and the red dots shows the transverse fluctuations. Red dashed line is $t^{3/4}$ and blue dashed line is $t^{7/8}$ as predicted by [39].

4.2 Crosslinkers

Crosslinker proteins dynamically connect actin filaments, thereby propagating force from one to another. Thus model crosslinkers, must be able to attach and detach from actin filaments, and be compliant in order to propagate force. They are therefore modeled as hookean springs, with stiffness k_{cl} and rest length l_{cl} . Like actin filaments, the Young's modulus of most crosslinkers is significantly higher than would be reasonable to simulate; therefore we set $k_{cl} = 1-100pN/\mu m$ was so that the bending mode of actin filaments was significantly softer than the stretching mode of crosslinkers. Their rest length l_{cl} differs by the type of cross-linker and ranges from $10nm$ for fascin to $150nm$ for filamin.

At each time step of the simulation an unattached crosslinker head is allowed to attach to nearby filaments and an attached crosslinker head can detach. The probability of a head

attaching to an actin filament is a Gaussian distributed random variable, such that

$$P_{cl}^{on} = k_{cl}^{on} dt \exp(-r^2/R^2) \quad (8)$$

where r is the shortest distance from the head to the actin filament and $R = \sqrt{\frac{2k_B T}{k_{cl}}}$ where k_B is Boltzmann's constant and T is the temperature. For crosslinker detachment we assume that the behavior is that of a slip bond, such that a higher tensile force along the crosslinker backbone will result in a higher probability of detachment. Thus,

$$P_{cl}^{off} = k_{cl}^{off} dt \exp(Fx_{cl}/k_B T) \quad (9)$$

where F is the force along the crosslinker backbone, and x_{cl} is a characteristic bond length [3].

When a crosslinker is bound to a filaments at both ends, it will necessarily be stretched or compressed. If it were allowed to relax independently of the actin filaments to which it is bound, it would no longer lie on those filaments. Therefore, the tensile force stored on a stretched or compressed crosslinker is propagated onto those actin filaments via the lever rule outlined in [14, 30]. Thus, if the tensile force of a motor at point r_j between filament beads i and $i + 1$ is F_{cl} , then,

$$\begin{aligned} F_i &= F_{cl} \left| \left(\frac{r_j - r_i}{r_{i+1} - r_i} \right) \right| \\ F_{i+1} &= F - F_i \end{aligned} \quad (10)$$

will be the forces on beads i and $i + 1$ respectively due to the crosslinker.

4.3 Motors

Within the cytoskeleton, tens of myosin II motors aggregate into bipolar ensembles called myosin minifilaments [3]. While the mechanochemical process through which individual myosin motors walk along actin filaments is complex, motility assay experiments have shown that on average bound myosin II heads walk at an unloaded speed of $v_0 \approx 1\mu m/s$ along actin filaments [40]. To a first approximation, minifilaments therefore should also have a mean speed of $1\mu m/s$ (although see [3] and [23] for higher order measurements). Since myosin also functions to increase the local elasticity of networks wherever it is bound, the myosin is modeled similarly to a crosslinker, in that it behaves like a hookean spring with two heads, a stiffness k_m and a rest length l_m . It should be noted, however, that the two heads of this spring do not correspond directly to individual molecular myosin heads; rather each of them represents tens of myosin molecules, and their rate constants will reflect that notion. It would be undesirable for a myosin minifilament to stretch, since experimentally they have a very high Young's modulus and it is unlikely that their length would change noticeably in the cytoskeleton. Thus we set $k_m \gg \kappa_B/l_a$ so that the bending of actin is still the softest mode. The rest length was set to the average length of minifilaments [41]. Attachment and detachment kinetics for motors are the same as for crosslinkers, subscripted with m instead of cl in Equations (8) and (9). One extra parameter is needed k_m^{end} for the detachment of myosin from the barbed end of a filament, as detachment from the end is significantly more probable than from the rest of the filament. Similarly, force propagation onto minifilaments is done using the lever rule described in Section 4.2.

Unlike crosslinkers, motors process towards the barbed end of actin filaments to which they are bound at speeds that vary depending on the tensile force along the crosslinker. The relationship between motor velocity and tensile force is modeled linearly, such that the motor

head will speed up if the minifilament is compressed (pre-powerstroke) and slow down if the minifilament is stretched (post powerstroke) going to 0 when the force on the minifilament is the stall force $F_s \approx 3.85pN$ [14, 30]; i.e.,

$$v(F_{||}) = v_0 \left(1 - \frac{F_{||}}{F_s} \right) \quad (11)$$

where $F_{||}$ is the force on the motor, projected along the tangent vector of the actin filaments. The minor differences between crosslinkers and motors allow us treat them equivalently, by setting $v_0 = 0$ for the crosslinkers.

4.4 Dynamics

We Langevin dynamics to solve for the motion of actin filaments, myosin minifilaments and crosslinkers. The Langevin equations of motion for a spherical bead of mass m and radius R at position $r(t)$ at time t can be written,

$$m\ddot{r}(t) = F(t) + B(t) - 4\pi R\nu\dot{r}(t) \quad (12)$$

where $F(t)$ is the force on the particle due to its interactions and $B(t)$ is Brownian forcing term, to simulate a temperature, ν is the dynamic viscosity of the bead's environment, and we have used the Einstein relation for the damping term. Since the fastest motion in this simulation is that of the myosin, and a $0.4\mu m$ myosin minifilament moving at a speed of $1\mu m/s$ in a liquid at least as viscous as water ($\nu_D = 10^6\mu m^2/s$ dynamic viscosity) has a very low Reynold's number ($Re \approx 4 * 10^{-7}$) we can treat the dynamics in the overdamped limit where the equation of motion is Equation (12) without the acceleration term, i.e. with $m = 0$. Furthermore, in the limit of small Δt , we may write $\dot{r}(t) \approx \frac{r(t+\Delta t) - r(t)}{\Delta t}$. These two approximations allow us to rewrite Equation (12) as

$$r(t + \Delta t) = r(t) + F(t)\mu\Delta t + B(t)\mu\Delta t \quad (13)$$

where $\mu = (4\pi R\nu)^{-1}$. For the Brownian term, we use the form of Leimkuhler and Matthews [42, 43] that has been shown to minimize deviations from canonical averages in harmonic systems,

$$B(t) = \sqrt{\frac{2k_B T}{\mu\Delta t}} \left(\frac{W(t) + W(t - \Delta t)}{2} \right) \quad (14)$$

where $W(t)$ is a Wiener process, in this case a random number drawn from the normal distribution with mean zero and standard deviation of unity.

4.5 Environment

Because the probability of motor attachment decays as a Gaussian function of distance from the filament, it would be highly inefficient to attempt motor attachments with every filament in the simulation. Rather, we choose to test for connections only within a cutoff distance $r_c > 3R/2$ (where R is defined above as in Equation (8)). A grid of lattice size $2r_c$ is drawn in the $2D$ plane of the simulation, and the position of a filament is approximated as the points on the grid nearest to the beads of the filament. Thus, to determine if a motor will bind to a filament at time t , it is sufficient to only attempt attachment to filaments that are indexed at the four nearest grid points to a motor.

In general, we use periodic boundary conditions so as to limit effects of a boundary and to mimic a system larger than the one we simulate. Lees-Edwards boundaries [22] were used for shearing simulations, and hard wall boundaries have also been implemented. The value for Δt in Equation (13) generally depends on both the unloaded myosin speed v_0 and the largest stiffness in the simulation k_f . For $k_f = 10\text{pN}/\mu\text{m}$ and $v_0 = 1\mu\text{m}/\text{s}$ a value of $\Delta t = 0.00001\text{s}$ was sufficiently low to solve Equation (13) for hundreds of seconds without spuriously generating configurations of very large energy. The length and width of the simulations were chosen so as to be high enough to avoid boundary artifacts. A complete list of simulation parameters used throughout this article is provided in Table 1.

5 Acknowledgements

We thank M. Gardel, J. Weare, C. Matthews, F. Nedelev, F. Mackintosh, and M. Murrell for helpful conversations. This research was supported in part by the University of Chicago Materials Research Science and Engineering Center (NSF Grant No. 1420709). S.L.F. was supported by the Department of Defense (DoD) through the National Defense Science & Engineering Graduate Fellowship (NDSEG) Program. G.M.H. was supported by an NIH Ruth L. Kirschstein NRSA award (1F32GM113415-01).

References

- [1] Michael P. Murrell and Margaret L. Gardel. F-actin buckling coordinates contractility and severing in a biomimetic actomyosin cortex. *Proceedings of the National Academy of Sciences*, 109(51):20820–20825, 2012.
- [2] H.E. Huxley. The mechanism of muscular contraction. *Science*, 164(3886):1356–1366, 1969.
- [3] Samantha Stam, Jon Alberts, Margaret L. Gardel, and Edwin Munro. Isoforms confer characteristic force generation and mechanosensation by myosin ii filaments. *Biophysical journal*, 108(8):1997–2006, 2015.
- [4] Michael Murrell, Patrick W. Oakes, Martin Lenz, and Margaret L. Gardel. Forcing cells into shape: the mechanics of actomyosin contractility. *Nature Reviews Molecular Cell Biology*, 16(8):486–498, 2015.
- [5] Michael Murrell and Margaret L. Gardel. Actomyosin sliding is attenuated in contractile biomimetic cortices. *Molecular Biology of the Cell*, 25(12):1845–1853, 2014.
- [6] M.L. Gardel, J.H. Shin, F.C. MacKintosh, L. Mahadevan, P. Matsudaira, and D.A. Weitz. Elastic behavior of cross-linked and bundled actin networks. *Science*, 304(5675):1301–1305, 2004.
- [7] Stanislav Burov, S.M. Ali Tabei, Toan Huynh, Michael P. Murrell, Louis H. Philipson, Stuart A. Rice, Margaret L. Gardel, Norbert F. Scherer, and Aaron R. Dinner. Distribution of directional change as a signature of complex dynamics. *Proceedings of the National Academy of Sciences*, 110(49):19689–19694, 2013.

- [8] F.C. MacKintosh, J. Käs, and P.A. Janmey. Elasticity of semiflexible biopolymer networks. *Physical Review Letters*, 75(24):4425, 1995.
- [9] D. A. Head, A. J. Levine, and F. C. MacKintosh. Distinct regimes of elastic response and deformation modes of cross-linked cytoskeletal and semiflexible polymer networks. *Phys. Rev. E*, 68:061907, Dec 2003.
- [10] Jan Wilhelm and Erwin Frey. Elasticity of stiff polymer networks. *Physical Review Letters*, 91(10):108103, 2003.
- [11] Taeyoon Kim, Wonmuk Hwang, Hyungsuk Lee, and Roger D. Kamm. Computational analysis of viscoelastic properties of crosslinked actin networks. 2009.
- [12] Francois Nedelec and Dietrich Foethke. Collective langevin dynamics of flexible cytoskeletal fibers. *New Journal of Physics*, 9(11):427, 2007.
- [13] Thorsten Erdmann and Ulrich S. Schwarz. Stochastic force generation by small ensembles of myosin ii motors. *Physical Review Letters*, 108(18):188101, 2012.
- [14] Daniel Gordon, Anne Bernheim-Grosbasser, Chen Keasar, and Oded Farago. Hierarchical self-organization of cytoskeletal active networks. *Physical Biology*, 9(2):026005, 2012.
- [15] Shenshen Wang and Peter G. Wolynes. Active contractility in actomyosin networks. *Proceedings of the National Academy of Sciences*, 109(17):6446–6451, 2012.
- [16] Nilushi L. Dasanayake, Paul J. Michalski, and Anders E. Carlsson. General mechanism of actomyosin contractility. *Physical Review Letters*, 107(11):118101, 2011.
- [17] Taeyoon Kim. Determinants of contractile forces generated in disorganized actomyosin bundles. *Biomechanics and modeling in mechanobiology*, 14(2):345–355, 2014.
- [18] Hajar Ennmani, Gaëlle Letort, Christophe Guérin, Jean-Louis Martiel, Wenxiang Cao, François Nédélec, M Enrique, Manuel Théry, and Laurent Blanchoin. Architecture and connectivity govern actin network contractility. *Current Biology*, 26(5):616–626, 2016.
- [19] Yi-Chia Lin, Norman Y. Yao, Chase P. Broedersz, Harald Herrmann, Fred C. MacKintosh, and David A. Weitz. Origins of elasticity in intermediate filament networks. *Physical Review Letters*, 104(5):058101, 2010.
- [20] KE Kasza, GH Koenderink, YC Lin, CP Broedersz, W Messner, F Nakamura, TP Stossel, FC MacKintosh, and DA Weitz. Nonlinear elasticity of stiff biopolymers connected by flexible linkers. *Physical Review E*, 79(4):041928, 2009.
- [21] Denis J. Evans and G.P. Morriss. Nonlinear-response theory for steady planar couette flow. *Physical Review A.*, 30(3):1528, 1984.
- [22] Mike P. Allen and Dominic J. Tildesley. *Computer simulation of liquids*. Oxford university press, 1989.
- [23] Sam Walcott, David M. Warshaw, and Edward P. Debold. Mechanical coupling between myosin molecules causes differences between ensemble and single-molecule measurements. *Biophysical journal*, 103(3):501–510, 2012.

- [24] David E. Harris and D.M. Warshaw. Smooth and skeletal muscle myosin both exhibit low duty cycles at zero load in vitro. *Journal of Biological Chemistry*, 268(20):14764–14768, 1993.
- [25] Seiji Umemoto and James R Sellers. Characterization of in vitro motility assays using smooth muscle and cytoplasmic myosins. *Journal of Biological Chemistry*, 265(25):14864–14869, 1990.
- [26] BA DiDonna and Alex J Levine. Unfolding cross-linkers as rheology regulators in f-actin networks. *Physical Review E*, 75(4):041909, 2007.
- [27] F. Gittes and F.C. MacKintosh. Dynamic shear modulus of a semiflexible polymer network. *Physical Review E*, 58(2):R1241, 1998.
- [28] Kei W Müller, Robijn F Bruinsma, Oliver Lieleg, Andreas R Bausch, Wolfgang A Wall, and Alex J Levine. Rheology of semiflexible bundle networks with transient linkers. *Physical review letters*, 112(23):238102, 2014.
- [29] Jeffrey Vieregg, Michael Lueckheide, Lorraine Leon, Amanda Marciel, and Matthew Tirrell. Nucleic acid-peptide complex phase controlled by dna hybridization. *Bulletin of the American Physical Society*, 2016.
- [30] François Nédélec. Computer simulations reveal motor properties generating stable antiparallel microtubule interactions. *The Journal of Cell Biology*, 158(6):1005–1015, 2002.
- [31] Taeyoon Kim, W Hwang, and RD Kamm. Computational analysis of a cross-linked actin-like network. *Experimental Mechanics*, 49(1):91–104, 2009.
- [32] Monika Scholz, Stanislav Burov, Kimberly L Weirich, Björn J Scholz, SM Ali Tabei, Margaret L Gardel, and Aaron R Dinner. Cycling state that can lead to glassy dynamics in intracellular transport. *Physical Review X*, 6(1):011037, 2016.
- [33] M. Murrell. personal communication.
- [34] Theo Odijk. The statistics and dynamics of confined or entangled stiff polymers. *Macromolecules*, 16(8):1340–1344, 1983.
- [35] Michael Rubinstein and Ralph H. Colby. *Polymer Physics*. OUP Oxford, 2003.
- [36] H. Kojima, A. Ishijima, and T. Yanagida. Direct measurement of stiffness of single actin filaments with and without tropomyosin by in vitro nanomanipulation. *Proceedings of the National Academy of Sciences*, 91(26):12962–12966, 1994.
- [37] Hideo Higuchi, Toshio Yanagida, and Yale E. Goldman. Compliance of thin filaments in skinned fibers of rabbit skeletal muscle. *Biophysical Journal*, 69(3):1000, 1995.
- [38] C. Frontali, E. Dore, A. Ferrauto, E. Gratton, A. Bettini, M.R. Pozzan, and E. Valdevit. An absolute method for the determination of the persistence length of native dna from electron micrographs. *Biopolymers*, 18(6):1353–1373, 1979.
- [39] R. Everaers, F. Jülicher, A. Ajdari, and A.C. Maggs. Dynamic fluctuations of semiflexible filaments. *Physical Review Letters*, 82(18):3717, 1999.

- [40] Jeffrey T. Finer, Robert M. Simmons, James A. Spudich, et al. Single myosin molecule mechanics: piconewton forces and nanometre steps. *Nature*, 368(6467):113–119, 1994.
- [41] Richard Niederman and Thomas D. Pollard. Human platelet myosin. ii. in vitro assembly and structure of myosin filaments. *The Journal of Cell Biology*, 67(1):72–92, 1975.
- [42] Benedict Leimkuhler and Charles Matthews. Rational construction of stochastic numerical methods for molecular sampling. *Applied Mathematics Research eXpress*, page abs010, 2012.
- [43] Benedict Leimkuhler and Charles Matthews. Robust and efficient configurational molecular sampling via langevin dynamics. *The Journal of Chemical Physics*, 138(17):174102, 2013.
- [44] A. Ott, M. Magnasco, A. Simon, and A. Libchaber. Measurement of the persistence length of polymerized actin using fluorescence microscopy. *Physical Review E*, 48(3):R1642, 1993.
- [45] Stephen J. Kron and James A. Spudich. Fluorescent actin filaments move on myosin fixed to a glass surface. *Proceedings of the National Academy of Sciences*, 83(17):6272–6276, 1986.
- [46] Claudia Veigel, Justin E. Molloy, Stephan Schmitz, and John Kendrick-Jones. Load-dependent kinetics of force production by smooth muscle myosin measured with optical tweezers. *Nature Cell Biology*, 5(11):980–986, 2003.
- [47] Jorge M. Ferrer, Hyungsuk Lee, Jiong Chen, Benjamin Pelz, Fumihiko Nakamura, Roger D. Kamm, and Matthew J. Lang. Measuring molecular rupture forces between single actin filaments and actin-binding proteins. *Proceedings of the National Academy of Sciences*, 105(27):9221–9226, 2008.
- [48] Jonathan Stricker, Tobias Falzone, and Margaret L. Gardel. Mechanics of the f-actin cytoskeleton. *Journal of biomechanics*, 43(1):9–14, 2010.

6 Supplement

6.1 Algorithm Pseudocode

In pseudocode we can describe each timestep of the simulation as follows

```

For Each Bead on Each Filament:
    Update force from filament stretching
    Update force from filament bending

    Update position via Equation (13)

For Each Head on each Motor (cross-linker)
    If head is unattached
        try to attach
        Add up forces (stretching)

    Update position via Equation (13)

```

```

If head is attached
    Update position via Equation (13)
    Try to detach
    If not detached
        Step toward barbed end
        Update attached actin with stretch force
Update neighbor lists

```

6.2 Further tests of the WLC model

From Equation (7) the distribution of the square of end to end distances can be calculated as

$$\langle r^2 \rangle = \int_0^L ds' \int_0^L ds \exp(|s - s'|)/(2L_p) = 4L_p L \left(1 - \frac{2L_p}{L} (1 - \exp(-L/2L_p)) \right) \quad (15)$$

Thus, Equation (15) provides a third method for measuring the persistence length by averaging the observable $r_N - r_0$. Figure S1(d) shows the results of the end to end distributions for each of these sets of simulations for each L . We fit this data to Equation (15) to obtain a third estimate for L_p . See Section 6.2 for further detail regarding the calculation of data points, error bars, and fits in these plots. The agreement between the three fits in Figure 8(B) and Figure S1(d), and the fact that all measurements produced data in reasonable correspondance with the input persistence length, $L_p = \kappa_B/k_B T = 20\mu m$ show that the model correctly simulates a semiflexible filament. In Figure 8(B), for each value of L , the results of the 10 simulations were averaged to give one number $\overline{\theta_L^2(l)}$, and a standard deviation $\sigma(\overline{\theta_L^2(l)})$. These values were then averaged to obtain a single value of $\overline{\theta^2(l)} = \sigma(\theta^2(l))^2 \sum_L \frac{\overline{\theta_L^2(l)}}{\sigma(\overline{\theta_L^2(l)})^2}$ where $\sigma(\theta^2(l))^2 = 1/\sum_L \sigma(\overline{\theta_L^2(l)})^{-2}$. The values for the $\overline{\theta^2(l)}$ were fit to a line via least squares and L_p was calculated as the inverse of the slope. The same process was done for the data points in the blue curve, wherein $\ln((\cos(\theta(l)))$ was fit to a line via least squares and $L_p = -1/2m$ where m is the slope of the fit line. For Figure S1(d), the data point itself is the average of $\langle r^2(L) \rangle$ over the 10 simulations, and the error bars show one standard deviation of the ensemble. The data is then fit to the nonlinear function in Equation (15) using the *Wolfram Mathematica* function *NonlinearModelFit* and a value for L_p is predicted.

6.2.1 Further tests of the WLC model

To verify that the persistence length was independent of the stretching stiffness k_f , we evaluated L_p using a fit to Equation (7) for various values of k_a as shown in Figure S1(b). For $k_a > 5pN/\mu m$ we find that L_p is independent of k_a .

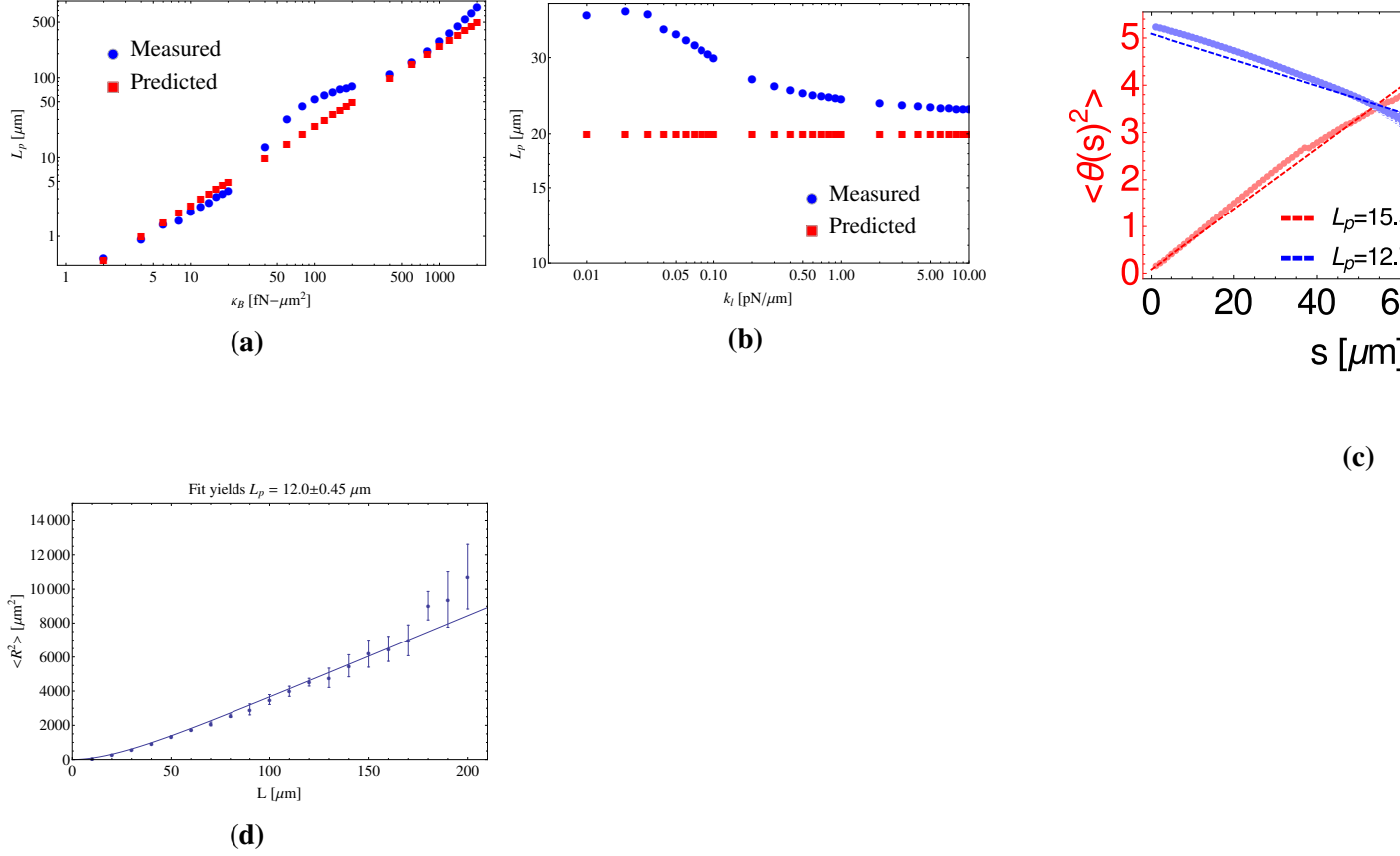


Figure S1: (a) Input bending modulus vs measured persistence length over three orders of magnitude. Persistence length was measured by fitting a line to $\ln(\langle \cos(\theta) \rangle)$ in each case. (b) Persistence length as function of stretching stiffness approaches correct answer for high enough stiffness. (c) Methods 1 and 2 of measuring persistence length, described in main text using different length filaments. (d) A third method for measuring persistence length, as function of end to end distance, described above.

6.3 Strain Stiffening

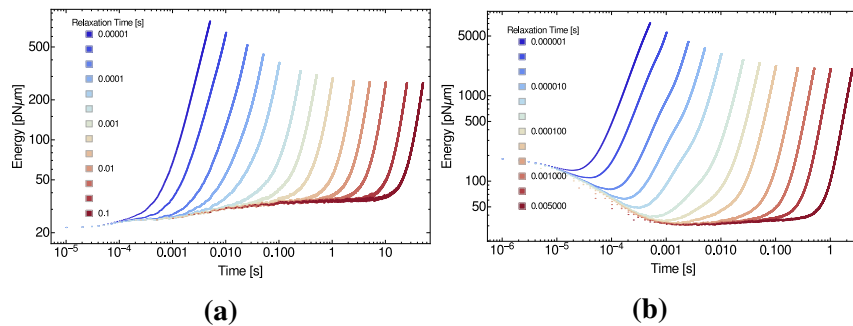


Figure S2: Strain energy as function of time for various relax times t_{relax} for networks with (a) $k_{cl} = 10$ pN/μm and (b) $k_{cl} = 100$ pN/μm crosslinked networks

6.4 Bundling

To contrast between bundling, contractility, and polarity sorting we computed the divergence of bundled networks, as well as the radial distribution function of the filament barbed ends in bundled networks. The results are shown in figure Figure S3.

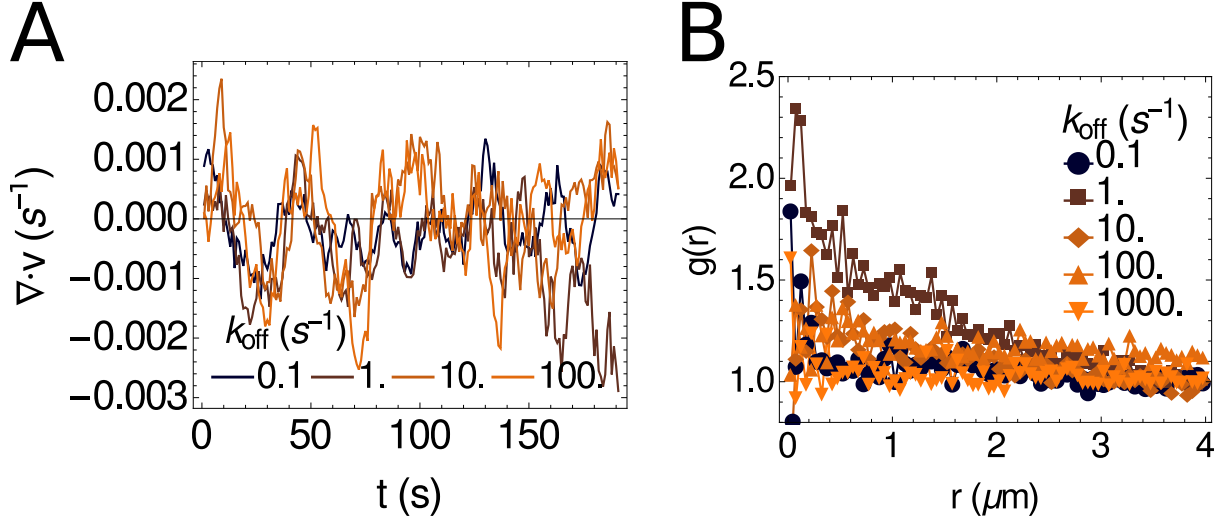


Figure S3: (A) Assemblies without motors that bundle do not show an average negative divergence, unlike assemblies with motors (Figure 6). (B) The radial distribution function for bundled networks for the barbed end of filaments is significantly less peaked than for all points on the filaments (Figure 2). Thus, the network is not polarity sorted.